ChemPubSoc Europe

DOI: 10.1002/chem.201502921

CHEMISTRY A European Journal Communication

Fluorescence |*Hot Paper*|

Near-Infrared Phosphorus-Substituted Rhodamine with Emission Wavelength above 700 nm for Bioimaging

Xiaoyun Chai,[a] Xiaoyan Cui,[b] Baogang Wang,[a] Fan Yang,[a, c] Yi Cai,[a, c] Qiuye Wu,[a] and Ting Wang*[a]

Abstract: Phosphorus has been successfully fused into a classic rhodamine framework, in which it replaces the bridging oxygen atom to give a series of phosphorus-substituted rhodamines (PRs). Because of the electron-accepting properties of the phosphorus moiety, which is due to effective σ^*–π^* interactions and strengthened by the inductivity of phosphine oxide, PR exhibits extraordinary long-wavelength fluorescence emission, elongating to the region above 700 nm, with bathochromic shifts of 140 and 40 nm relative to rhodamine and silicon-substituted rhodamine, respectively. Other advantageous properties of the rhodamine family, including high molar extinction coefficient, considerable quantum efficiency, high water solubility, pH-independent emission, great tolerance to photobleaching, and low cytotoxicity, stay intact in PR. Given these excellent properties, PR is desirable for NIR-fluorescence imaging in vivo.

Advances in chemistry, environmental science, biology, and medicine are often dependent on small-molecule fluorophores with tailored chemical and photophysical properties to be used as environmental indicators, biomolecular tags, or cellular stains.[1] Among the various fluorophores, the well-known xanthene dye rhodamine has found extensive use due to favorable characteristics, including high absorptivity, excellent fluorescence properties, great photostability, and tunability for probe design.[2] Although rhodamine is widely used in bioimaging, the applications are facing a daunting challenge: the absorption and emission wavelengths are typically below 600 nm, which are sometimes not suitable in vivo.[3] Many efforts have been made to obtain new rhodamine analogues with longer emission wavelengths, but retained advantages of the parent fluorophore. One efficient way is to perturb the skeleton of the xanthene core with other atoms, such as C,[4] Si,[5] Ge,[6] Se,[7] and Te.[8] In particular, replacement of the bridging oxygen atom with a silicon atom elicits a 90 nm bathochromic shift compared with the parent rhodamine, yielding near-infrared (NIR) Si-rhodamine with emission maximum at around 650 nm.[5] Nonetheless, this is still not favorable for practical bioimaging, because two longer wavelength windows at 700 nm and 800 nm with deeper tissue penetration and lower background fluorescence are often used.[9] More recently, Nagano and co-workers applied a ring-expansion strategy to the Si-rhodamine scaffold and obtained two NIR fluorescent dyes with the emission wavelength elongated to 700 nm.[10] Klán and co-workers synthesized 9-phenylethynyl Si-pyronine with an emission-wavelength maximum at 730 nm.[11] However, the proposed strategies stated above still have some disadvantages, such as restricted structural flexibility or diminished fluorescence quantum yield.

The fusion of main-group elements into rhodamine framework to replace the bridging oxygen atom has become an attractive research area, because the replacing atoms can effectively tune the chemical and photophysical properties of the fluorescent dye at the electronic level, resulting in a revolution of the traditional rhodamine.[5,12] Surprisingly, the replacing atoms have so far been mainly limited to groups 16 and 14 elements, whereas atoms in other groups have received little attention. We anticipate that fusing new groups of atom into the rhodamine framework might boost the development of rhodamine-inspired fluorophores with intriguing chemical and photophysical properties. Furthermore, it will provide more insights into the effects exerted by the replacing atoms.

Organophosphorus species have attracted great interest due to the unique optical and electronic features.[13] Phosphorus offers a peculiar geometry, which gives rise to σ^*–π^* orbital coupling when incorporated within conjugated ring systems, altering the energy level of the LUMO. The electron-accepting properties of the phosphorus moiety can be further increased by phosphine oxides (P-oxides), which tune the chemical and photophysical properties. Because of these attractive features of the phosphorus moiety, phosphacyclic π-conjugated materials have been widely applied in organic light-emitting diodes,[14] organic photovoltaic cells,[15] and fluorescent probes.[16]

Inspired by the unique geometrical and electronic characteristics of phosphorus, we successfully fused a phosphorus atom into the rhodamine framework to replace the bridging oxygen

[a] *Dr. X. Chai, B. Wang, F. Yang, Y. Cai, Prof. Q. Wu, Dr. T. Wang*
Department of Organic Chemistry, College of Pharmacy
Second Military Medical University
Shanghai 200433 (P.R. China)
E-mail: wangting1983927@gmail.com

[b] *X. Cui*
Department of Chemistry, New York University
New York, New York 10003 (USA)

[c] *F. Yang, Y. Cai*
College of Pharmacy, Yantai University
Yantai, Shandong 264005 (P.R. China)

Supporting information for this article is available on the WWW under http://dx.doi.org/10.1002/chem.201502921.

atom and obtained a series of phosphorus-substituted rhodamines (PR, Scheme 1) with fluorescence emission extended into the region above 700 nm. To the best of our knowledge, this is the first example of a phosphorus-substituted rhodamine with distinctive long-wavelength NIR emission. Furthermore, we demonstrated the superior characteristics for in vivo imaging, including excellent NIR photophysical properties, high water solubility, great photostability, and low cytotoxicity.

Two approaches have been established to synthesize PR. The synthetic route is shown in Scheme 2 and the procedures are described in detail in the Supporting Information. Key intermediate bis(3-(diethylamino)phenyl)(methyl)phosphine oxide (NEt_2-MDPP) was synthesized from methyldiphenylphosphine (MDPP) by steps of nitration, reduction, and alkylation according to reported procedures.[17] The following coupling and oxidation afforded the phosphorus-containing xanthone (PX). In the ^{1}H NMR spectra, hydrogen atoms from the methyl group bonded to the phosphorus atom (P-Me) split into a doublet resonating at approximately $\delta = 2$ ppm with $J_{H-P} \approx 13$ Hz.[17,18] With NEt_2-MDPP and PX in hand, we designed and synthesized Me-PR by inserting 2-methyl phenyl at the 9-position of the xanthene core through a condensation process with NEt_2-MDPP[19] or a typical organometallic addition to PX.[5b] Both approaches lead to the desired product; the former through a simpler procedure and the later with higher yields. A green solid was obtained after purification through C18 semi-preparative liquid chromatography. As exhibited in Figure 1, two sets of split doublets assigned as P-Me were found ($\delta = 1.95$ and 1.93 ppm, $J_{H-P} = 12.4$ Hz and 12.4 Hz, respectively). Furthermore, the ^{31}P NMR spectrum displays two neighboring peaks ($\delta = 15.55$ and 15.36 ppm), indicating the existence of two types of phosphorus atoms in the molecule. The NMR results clearly suggested that Me-PR exists in two stereoisomers: the *cis* form (two methyl moieties, one with methyl bonded to the phosphorus and the other bonded to the phenyl ring, are on the same side of the plane defined by the phosphorus replaced xanthene group) and the *trans* form (the two methyl groups on opposite sides). HPLC analyses further demonstrated that two isomers were present at the ratio of approximately 1:1 (Figure S1 and S2 in the Supporting Information). Great efforts have been devoted to separate the two isomers. Unfortunately the separation failed due to extremely similar structures and polarities. To avoid isomerization, symmetric PRs, with no methyl substitution and tMe-PR with 2′,4′,6′-trimethyl substitution were designed, synthesized and characterized as stereoisomerically pure PRs. Meanwhile, the oxygen and silicon rhodamine analogues (Me-OR and Me-SiR; see the Supporting Information) were also prepared for comparison. All new compounds were characterized by mass spectrometry and NMR spectroscopy.

Figure S3 in the Supporting Information shows the colors and Figure 2 gives the absorption and emission spectra of the PRs, as well as the congeners Me-OR and Me-SiR in PBS at pH 7.4. The solutions of Me-OR, Me-SiR, and Me-PR are red, blue, and light green, respectively. Although the profile of the absorption spectra were very similar, the PRs exhibit large redshifts, producing bathochromic shifts of 140 and 40 nm compared with Me-OR and Me-SiR, respectively. The UV spectra obtained from the HPLC analysis show that the absorption of the two Me-PR isomers matched well, indicating similar spectral properties (Figure S1 in the Supporting Information). All PRs exhibit emission maxima at about 710 nm, undergoing a similar redshift trend. Detailed photophysical properties of the PRs in different media are summarized in Table 1 (Figures S4–S6 in Supporting Information). In the same solvent, different PRs have similar absorption (λ_{abs}) and emission maxima (λ_{em}), suggesting that methyl substitution exerted negligible impact on the spectral features. However, the fluorescence quantum efficiency (Φ_f) improved with increasing number of methyl substituents, because of the reduction of energy loss by restricted rotation. In the series of PRs, the maximum absorption and emission in PBS and ethanol underwent a moderate redshift (ca. 10 nm) relative to those in acetonitrile and dichloromethane. This shift is ascribed to the polarity of solvent, which in turn has a negative impact on fluorescence quantum efficiency

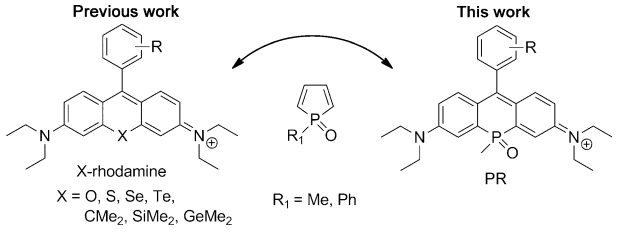

Scheme 1. The design strategy for PR.

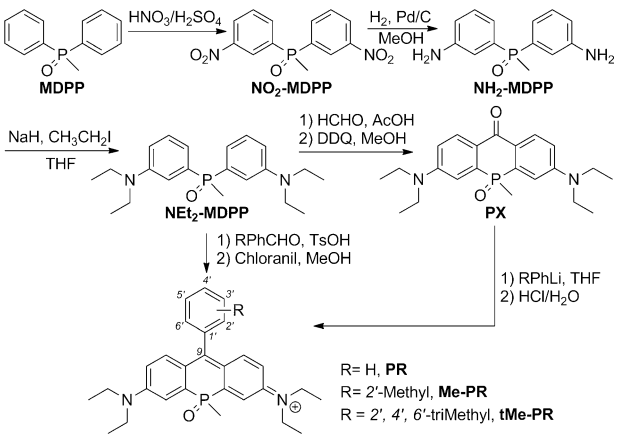

Scheme 2. Synthesis of PRs (DDQ = 2,3-dichloro-5,6-dicyano-1,4-benzoquinone; TsOH = *p*-toluenesulfonic acid).

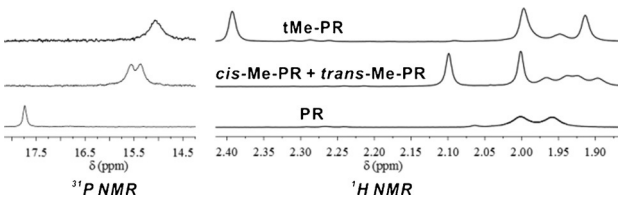

Figure 1. Partial ^{1}H NMR and ^{31}P NMR spectra of PRs.

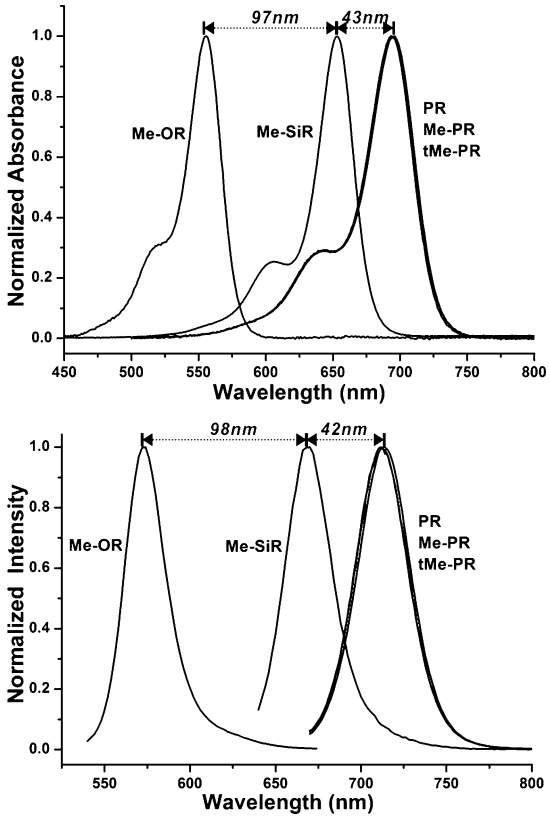

Figure 2. The absorption and emission spectra of Me-OR, Me-SiR, and the PRs in PBS at pH 7.4.

Table 1. The spectral properties of **PR**s in different solvents.[a]

Dyes	Solvent	λ_{abs} [nm]	ε [M^{-1} cm^{-1}]	λ_{em} [nm]	Φ_f[b]
PR	DCM	688	9.0×10^4	702	0.15
	MeCN	682	9.2×10^4	700	0.14
	EtOH	690	–	709	–
	PBS[b]	694	6.5×10^4	712	0.06
Me-PR[c]	DCM	688	1.1×10^5	702	0.36
	MeCN	684	9.8×10^4	700	0.26
	EtOH	691	6.6×10^4	709	0.11
	PBS[b]	694	9.2×10^4	712	0.11
tMe-PR	DCM	687	9.2×10^4	703	0.42
	MeCN	684	7.1×10^4	702	0.27
	EtOH	691	1.0×10^5	710	0.20
	PBS[b]	696	6.8×10^4	713	0.15

[a] Measured in solution containing 1% DMSO. [b] Quantum yields determined with reference Cy5.5 as standard ($\Phi_f = 0.23$ in PBS). [c] Determined with isomer mixtures without isolation.

of PRs. Me-PR and tMe-PR exhibited high molar extinction coefficient and considerable fluorescence quantum efficiency for further applications as NIR fluorescence dyes.

To further evaluate the electronic effects of phosphorus on the photophysical properties of PR, we performed time-dependent (TD) DFT calculations for Me-PR and the congeners by using Becke's parameter exchange functional, the LYP correlation functional, and Pople's double zeta basis with both diffuse and polarization functions (B3LYP/6-31 + G(d)).[20] As shown in

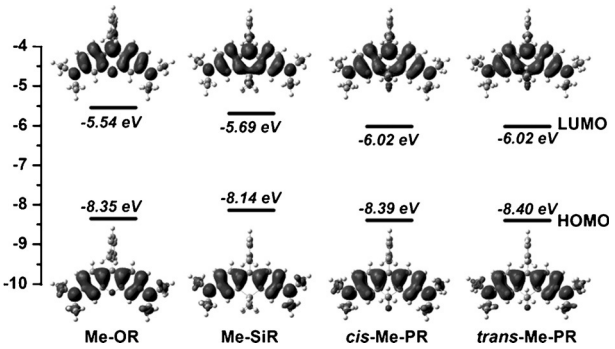

Figure 3. Computed frontier orbitals and energy levels of the dyes Me-OR, Me-SiR, *cis*-Me-PR, and *trans*-Me-PR with isodensity = 0.2.

Figure 3, the HOMO was spread over the entire π system in each dye, whereas the LUMO resides partially on the bridging atom; this shows a partial charge-transfer feature for the excited state. Particularly, the LUMO in Me-PR is shared with the electrons on the P-oxide moiety. This distribution of the LUMOs in Me-PR is a result from the inductive effects of the P-oxide moiety, which can accept the excited electrons from the conjugated π system. The intramolecular charge transfer stabilized the excited state of Me-PR and lowered the LUMO energy level. Moreover, the effective σ^*–π^* orbital interactions between P–Me, P=O and the fluorophore further lowered the energy of the LUMO of Me-PR, leading to the lowest LUMO energy level in the dyes.[21] The theoretical study also showed that the absorptions were crucially determined by the HOMO–LUMO transition (Table S1 in Supporting Information). The HOMO–LUMO energy gaps were 2.37, 2.38, 2.46, and 2.82 eV for ***cis***-Me-PR, *trans*-Me-PR, Me-SiR, and Me-OR, respectively; these values correlate well with the bathochromic shifts observed in the spectra. The two isomers of Me-PR, *cis*-Me-PR, and *trans*-Me-PR exhibited similar HOMO and LUMO shapes and orbital energy levels, indicating that they possess similar photophysical properties. Overall, the electron-accepting capability of the phosphorus moiety, which is mainly caused by the σ^*–π^* interactions and inductivity of the phosphine oxide, largely lowers the energy level of the LUMO, thus significantly narrows the HOMO–LUMO gaps. As a manifestation, the absorption and emission of PRs are substantially redshifted.

Considering the promising application of PRs in vivo, the properties were scrupulously evaluated. Firstly, we examined the spectral properties of PRs at different pH values in PBS. As shown in Figure S7 in the Supporting Information, the PRs keep the green color and constant strong fluorescence over a wide pH range from pH 2 to 12, confirming the pH-independent emission of the PRs at wide pH range. Photostability is crucial for fluorescent dyes, because it ensures prolonged observation. We further investigated the photobleaching tolerance of the PRs. Figure S8 in the Supporting Information shows the change in emission of the PRs upon light irradiation. Cy5.5, which is widely used as a labeling agent in vivo, was also examined for comparison, because it has similar spectral regions of absorption and emission as the PRs. Cy5.5 underwent obvious diminution of the emission upon light irradia-

tion. In contrast, Me-PR and tMe-PR exhibited no noticeable changes in the emission intensity under the same conditions, suggesting that Me-PR and tMe-PR have excellent photostability similar to that of the rhodamine and Si-rhodamine congeners.[22] Additionally, MTT (3-(4,5-dimethyl-2-thiazolyl)-2,5-diphenyl-2*H*-tetrazolium bromide) assays revealed that the cell viabilities of HepG2 cells were not noticeably affected by incubation with 1–10 μM of the PRs for 24 h, demonstrating low cytotoxicity (Figure S9 in Supporting Information). These results suggest that Me-PR and tMe-PR possess superior properties and are expected to serve as excellent fluorescent dyes for bioimaging in vivo.

To evaluate the capability of PRs in NIR bioimaging, Me-PR and tMe-PR were applied to stain living HepG2 cells and normal mice. PR can be readily loaded into living cells without any further modification, confirming similar membrane permeability to parent rhodamine. Figure 4 shows the red fluorescence inside the cells stained with tMe-PR (Figure S10 in the Supporting Information). Aqueous solutions of Me-PR and tMe-PR were further injected into the leg muscles of mice. Figure 5 shows the in vivo fluorescent images obtained at 0, 6, 24, and 48 h after intramuscular injection of tMe-PR (Figure S11 in the Supporting Information). After excitation, tMe-PR gave a strong NIR fluorescence emission, easily penetrating tissues with high signal-to-noise ratio. The fluorescence intensity gradually decayed with time because of diffusion and metabolism. Notably, a reliable fluorescence signal was still observed at the site of injection even after two days.

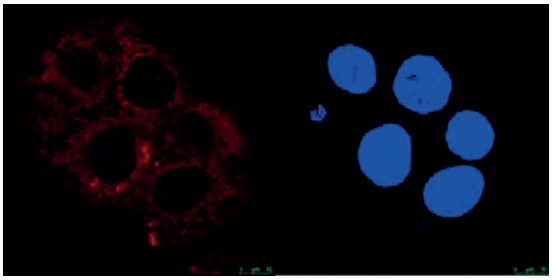

Figure 4. Fluorescence images of HepG-2 cells stained with 5 μM tMe-PR (left) and DAPI (right).

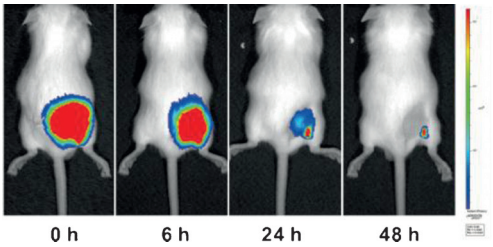

Figure 5. Time-dependent in vivo fluorescence images of mice after intramuscular injection of 100 μL tMe-PR (500 μg mL^{-1}).

In conclusion, we have successfully developed a series of phosphorus-substituted rhodamines by replacing the bridging oxygen atom with phosphorus. The fluorescence emission show bathochromic shifts of 140 and 40 nm relative to rhodamine and Si-rhodamine, respectively, owing to the electron-accepting character of the phosphorus moiety. We also demonstrate that the PRs can be used for practical in vivo imaging due to superior characteristics, such as NIR emission extended into the region above 700 nm, high molar extinction coefficient, sufficiently large quantum efficiency, high water solubility, pH-independent emission, great tolerance to photobleaching, and low toxicity. The construction of PR provides the prospect of multicolor imaging and NIR-fluorescent probe design. Experiments focusing on applications of this new fluorophore are currently underway and will be published in due course.

Acknowledgements

This work was supported by the National Natural Science Foundation of China (No. 21205135). We sincerely thank Prof. Bart Kahr at New York University for the use of Gaussian. We are also very grateful for the assistance of Dr. Yongle Li from Shanghai University and Prof. Kenjiro Hanaoka from the University of Tokyo.

Keywords: bioimaging · near-infrared · phosphorus · redshifted emission · rhodamine

[1] a) L. D. Lavis, R. T. Raines, *ACS Chem. Biol.* **2014**, *9*, 855 – 866; b) J. Chan, S. C. Dodani, C. J. Chang, *Nat. Chem.* **2012**, *4*, 973 – 984; c) Z. Liu, L. D. Lavis, E. Betzig, *Mol. Cell* **2015**, *58*, 644 – 659; d) Y. Yang, Q. Zhao, W. Feng, F. Li, *Chem. Rev.* **2013**, *113*, 192 – 270; e) X. Li, X. Gao, W. Shi, H. Ma, *Chem. Rev.* **2014**, *114*, 590 – 659.

[2] a) M. Beija, C. A. M. Afonso, J. M. G. Martinho, *Chem. Soc. Rev.* **2009**, *38*, 2410 – 2433; b) H. N. Kim, M. H. Lee, H. J. Kim, J. S. Kim, J. Yoon, *Chem. Soc. Rev.* **2008**, *37*, 1465 – 1472; c) X. Chen, T. Pradhan, F. Wang, J. S. Kim, J. Yoon, *Chem. Rev.* **2012**, *112*, 1910 – 1956.

[3] a) L. Yuan, W. Y. Lin, Y. T. Yang, H. Chen, *J. Am. Chem. Soc.* **2012**, *134*, 1200 – 1211; b) L. Yuan, W. Y. Lin, K. B. Zheng, L. W. He, W. M. Huang, *Chem. Soc. Rev.* **2013**, *42*, 622 – 661.

[4] a) J. B. Grimm, A. J. Sung, W. R. Legant, P. Hulamm, S. M. Matlosz, E. Betzig, L. D. Lavis, *ACS Chem. Biol.* **2013**, *8*, 1303 – 1310; b) K. Kolmakov, V. N. Belov, C. A. Wurm, B. Harke, M. Leutenegger, C. Eggeling, S. W. Hell, *Eur. J. Org. Chem.* **2010**, 3593 – 3610.

[5] a) M. Fu, Y. Xiao, X. Qian, D. Zhao, Y. Xu, *Chem. Commun.* **2008**, 1780 – 1782; b) Y. Kushida, T. Nagano, K. Hanaoka, *Analyst* **2015**, *140*, 685 – 695; c) G. Lukinavičius, K. Umezawa, N. Olivier, A. Honigmann, G. Yang, T. Plass, V. Mueller, L. Reymond, I. R. Corrêa Jr, Z.-G. Luo, C. Schultz, E. A. Lemke, P. Heppenstall, C. Eggeling, S. Manley, K. Johnsson, *Nat. Chem.* **2013**, *5*, 132 – 139; d) T. Wang, Q.-J. Zhao, H.-G. Hu, S.-C. Yu, X. Liu, L. Liu, Q.-Y. Wu, *Chem. Commun.* **2012**, *48*, 8781 – 8783.

[6] Y. Koide, Y. Urano, K. Hanaoka, T. Terai, T. Nagano, *ACS Chem. Biol.* **2011**, *6*, 600 – 608.

[7] a) Y. Ichikawa, M. Kamiya, F. Obata, M. Miura, T. Terai, T. Komatsu, T. Ueno, K. Hanaoka, T. Nagano, Y. Urano, *Angew. Chem. Int. Ed.* **2014**, *53*, 6772 – 6775; *Angew. Chem.* **2014**, *126*, 6890 – 6893; b) M. R. Detty, P. N. Prasad, D. J. Donnelly, T. Ohulchanskyy, S. L. Gibson, R. Hilf, *Bioorg. Med. Chem.* **2004**, *12*, 2537 – 2544.

[8] a) Y. Koide, M. Kawaguchi, Y. Urano, K. Hanaoka, T. Komatsu, M. Abo, T. Terai, T. Nagano, *Chem. Commun.* **2012**, *48*, 3091 – 3093; b) B. Calitree, D. J. Donnelly, J. J. Holt, M. K. Gannon, C. L. Nygren, D. K. Sukumaran, J. Autschbach, M. R. Detty, *Organometallics* **2007**, *26*, 6248 – 6257; c) M. W. Kryman, G. A. Schamerhorn, K. Yung, B. Sathyamoorthy, D. K. Sukumaran, T. Y. Ohulchanskyy, J. B. Benedict, M. R. Detty, *Organometallics* **2013**, *32*, 4321 – 4333.

[9] a) J. V. Frangioni, *Curr. Opin. Chem. Biol.* **2003**, *7*, 626 – 634; b) X. Shu, A. Royant, M. Z. Lin, T. A. Aguilera, V. Lev-Ram, P. A. Steinbach, R. Y. Tsien, *Science* **2009**, *324*, 804 – 807.

[10] Y. Koide, Y. Urano, K. Hanaoka, W. Piao, M. Kusakabe, N. Saito, T. Terai, T. Okabe, T. Nagano, *J. Am. Chem. Soc.* **2012**, *134*, 5029 – 5031.

[11] T. Pastierik, P. Šebej, J. Medalová, P. Štacko, P. Klán, *J. Org. Chem.* **2014**, *79*, 3374 – 3382.

[12] a) Y.-Q. Sun, J. Liu, X. Lv, Y. Liu, Y. Zhao, W. Guo, *Angew. Chem. Int. Ed.* **2012**, *51*, 7634 – 7636; *Angew. Chem.* **2012**, *124*, 7752 – 7754; b) K. Umezawa, D. Citterio, K. Suzuki, *Anal. Sci.* **2014**, *30*, 327 – 349; c) J. Fernández-Lodeiro, M. F. Pinatto-Botelho, A. A. Soares-Paulino, A. C. Gonçalves, B. A. Sousa, C. Princival, A. A. Dos Santos, *Dyes Pigm.* **2014**, *110*, 28 – 48.

[13] a) M. Stolar, T. Baumgartner, *Chem. Asian J.* **2014**, *9*, 1212 – 1225; b) T. Baumgartner, R. Reau, *Chem. Rev.* **2006**, *106*, 4681 – 4727; c) T. Baumgartner, *Acc. Chem. Res.* **2014**, *47*, 1613 – 1622.

[14] D. Joly, D. Tondelier, V. Deborde, W. Delaunay, A. Thomas, K. Bhanuprakash, B. Geffroy, M. Hissler, R. Réau, *Adv. Funct. Mater.* **2012**, *22*, 567 – 576.

[15] Y. Matano, A. Saito, Y. Suzuki, T. Miyajima, S. Akiyama, S. Otsubo, E. Nakamoto, S. Aramaki, H. Imahori, *Chem. Asian J.* **2012**, *7*, 2305 – 2312.

[16] a) X. He, P. Zhang, J.-B. Lin, H. V. Huynh, S. E. Navarro Muñoz, C.-C. Ling, T. Baumgartner, *Org. Lett.* **2013**, *15*, 5322 – 5325; b) X. He, A. Y. Y. Woo, J. Borau-Garcia, T. Baumgartner, *Chem. Eur. J.* **2013**, *19*, 7620 – 7630; c) E. Yamaguchi, C. Wang, A. Fukazawa, M. Taki, Y. Sato, T. Sasaki, M. Ueda, N. Sasaki, T. Higashiyama, S. Yamaguchi, *Angew. Chem. Int. Ed.* **2015**, *54*, 4539 – 4543; *Angew. Chem.* **2015**, *127*, 4622 – 4626; d) X.-D. Jiang, J. Zhao, D. Xi, H. Yu, J. Guan, S. Li, C.-L. Sun, L.-J. Xiao, *Chem. Eur. J.* **2015**, *21*, 6079 – 6082.

[17] B. Tan, C. N. Tchatchoua, L. Dong, J. E. McGrath, *Polym. Adv. Technol.* **1998**, *9*, 84 – 93.

[18] I. Granoth, Y. Sagall, H. Leader, *J. Chem. Soc. Perkin Trans. 1* **1978**, 465 – 468.

[19] B. Wang, X. Chai, W. Zhu, T. Wang, Q. Wu, *Chem. Commun.* **2014**, *50*, 14374 – 14377.

[20] a) R. Ditchfield, W. J. Hehre, J. A. Pople, *J. Chem. Phys.* **1971**, *54*, 724 – 728; b) T. Clark, J. Chandrasekhar, G. W. Spitznagel, P. V. R. Schleyer, *J. Comput. Chem.* **1983**, *4*, 294 – 301; c) M. J. Frisch, J. A. Pople, J. S. Binkley, *J. Chem. Phys.* **1984**, *80*, 3265 – 3269; d) C. Lee, W. Yang, R. G. Parr, *Phys. Rev. B* **1988**, *37*, 785 – 789; e) A. D. Becke, *J. Chem. Phys.* **1993**, *98*, 5648 – 5652.

[21] Consensus has been reached regarding the $\sigma^*-\pi^*$ orbital interaction and inductive effects of phosphine oxides in five membered phosphole units. Indiscriminately applying the conclusions from five-membered phospholes into the six-membered ring in our system is improper. However, $\sigma^*-\pi^*$ orbital couplings, including P–Me and P=O, in six-membered rings are made possible through the tetrahedral geometry of the P center (X. He, J-B Lin, W. H. K an, T. Baumgartner, *Angew. Chem. Int. Ed.* **2013**, *52*, 8990 – 8994; *Angew. Chem.* **2013**, *125*, 9160 – 9164), which is similar to the pyramidal geometry of phosphorus in five-membered phosphole units. Moreover, the phosphine oxide in our case is likely to have inductive effect as in the five-membered phosphole system. Thus, based on the peculiar geometrical and electronic characteristics of this phosphorus moiety, we conclude that $\sigma^*-\pi^*$ orbital interaction and inductive effects should both be valid, although direct evidence is absent in our six-membered ring system.

[22] T. E. McCann, N. Kosaka, Y. Koide, M. Mitsunaga, P. L. Choyke, T. Nagano, Y. Urano, H. Kobayashi, *Bioconjugate Chem.* **2011**, *22*, 2531 – 2538.

Received: July 24, 2015
Published online on September 30, 2015